Skeletal muscle sarcomeric SHG patterns photo-conversion by femtosecond infrared laser

Gaëlle Recher,[1] Denis Rouède,[2] Emmanuel Schaub,[1] and François Tiaho[1,*]

[1]*Université de Rennes1, Université européenne de Bretagne, UMR CNRS 6026, Campus de Beaulieu, 35042 Rennes Cedex, France*

[2]*Université de Rennes1, Université européenne de Bretagne, UMR CNRS 6251, Institut de Physique de Rennes, Campus de Beaulieu, 35042 Rennes Cedex, France*

**francois.tiaho@univ-rennes1.fr*

Abstract: Femtosecond laser at 780 nm excitation wavelength was used to photo-convert the physiological sarcomeric single band (SB) second harmonic generation (SHG) pattern into double band (DB) in *Xenopus laevis* premetamorphic tail muscles. This photo-conversion was found to be a third order non-linear optical process and was drastically reduced at 940 nm excitation wavelength. This effect was no longer observed in paraformaldehyde fixed muscles and was enhanced by hydrogen peroxide. The action of hydrogen peroxide suggests that reactive oxygen species (ROS) could contribute to this photo-conversion. These results demonstrate that sarcomeric DB SHG pattern is a marker of sarcomere photodamage in xenopus tadpole muscles and highlight the need of being very careful at using two-photon excitation while observing living tissues. Moreover they open new avenues for *in situ* intravital investigation of oxidative stress effects in muscle dysfunctions and diseases.

OCIS codes: (180.4315) Nonlinear microscopy; (190.4160) Multiharmonic generation; (170.0170) Medical optics and biotechnology; (140.3330) Laser damage.

References and links

1. P. J. Campagnola, A. C. Millard, M. Terasaki, P. E. Hoppe, C. J. Malone, and W. A. Mohler, "Three-dimensional high-resolution second-harmonic generation imaging of endogenous structural proteins in biological tissues," Biophys. J. **82**(1), 493–508 (2002).
2. A. Hopt, and E. Neher, "Highly nonlinear photodamage in two-photon fluorescence microscopy," Biophys. J. **80**(4), 2029–2036 (2001).
3. H. J. Koester, D. Baur, R. Uhl, and S. W. Hell, "Ca2+ fluorescence imaging with pico- and femtosecond two-photon excitation: signal and photodamage," Biophys. J. **77**(4), 2226–2236 (1999).
4. M. Rubart, "Two-photon microscopy of cells and tissue," Circ. Res. **95**(12), 1154–1166 (2004).
5. W. R. Zipfel, R. M. Williams, and W. W. Webb, "Nonlinear magic: multiphoton microscopy in the biosciences," Nat. Biotechnol. **21**(11), 1369–1377 (2003).
6. W. Denk, J. H. Strickler, and W. W. Webb, """"Two-photon laser scanning fluorescence microscopy," Science (New York, N," Y **248**, 73–76 (1990).
7. K. Svoboda, D. W. Tank, and W. Denk, "Direct measurement of coupling between dendritic spines and shafts," Science **272**(5262), 716–719 (1996).
8. U. K. Tirlapur, and K. König, "Targeted transfection by femtosecond laser," Nature **418**(6895), 290–291 (2002).
9. U. K. Tirlapur, K. König, C. Peuckert, R. Krieg, and K. J. Halbhuber, "Femtosecond near-infrared laser pulses elicit generation of reactive oxygen species in mammalian cells leading to apoptosis-like death," Exp. Cell Res. **263**(1), 88–97 (2001).
10. M. A. Aon, S. Cortassa, E. Marbán, and B. O'Rourke, "Synchronized whole cell oscillations in mitochondrial metabolism triggered by a local release of reactive oxygen species in cardiac myocytes," J. Biol. Chem. **278**(45), 44735–44744 (2003).
11. W. G. Fisher, W. P. Partridge, Jr., C. Dees, and E. A. Wachter, "Simultaneous two-photon activation of type-I photodynamic therapy agents," Photochem. Photobiol. **66**(2), 141–155 (1997).
12. T. Boulesteix, E. Beaurepaire, M. P. Sauviat, and M. C. Schanne-Klein, "Second-harmonic microscopy of unstained living cardiac myocytes: measurements of sarcomere length with 20-nm accuracy," Opt. Lett. **29**(17), 2031–2033 (2004).
13. S. V. Plotnikov, A. C. Millard, P. J. Campagnola, and W. A. Mohler, "Characterization of the myosin-based source for second-harmonic generation from muscle sarcomeres," Biophys. J. **90**(2), 693–703 (2006).

#139325 - $15.00 USD Received 7 Dec 2010; revised 14 Jan 2011; accepted 14 Jan 2011; published 19 Jan 2011

14. C. Greenhalgh, N. Prent, C. Green, R. Cisek, A. Major, B. Stewart, and V. Barzda, "Influence of semicrystalline order on the second-harmonic generation efficiency in the anisotropic bands of myocytes," Appl. Opt. **46**(10), 1852–1859 (2007).
15. N. Prent, C. Green, C. Greenhalgh, R. Cisek, A. Major, B. Stewart, and V. Barzda, "Intermyofilament dynamics of myocytes revealed by second harmonic generation microscopy," J. Biomed. Opt. **13**(4), 041318 (2008).
16. F. Vanzi, M. Capitanio, L. Sacconi, C. Stringari, R. Cicchi, M. Canepari, M. Maffei, N. Piroddi, C. Poggesi, V. Nucciotti, M. Linari, G. Piazzesi, C. Tesi, R. Antolini, V. Lombardi, R. Bottinelli, and F. S. Pavone, "New techniques in linear and non-linear laser optics in muscle research," J. Muscle Res. Cell Motil. **27**(5-7), 469–479 (2006).
17. M. Both, M. Vogel, O. Friedrich, F. von Wegner, T. Künsting, R. H. A. Fink, and D. Uttenweiler, "Second harmonic imaging of intrinsic signals in muscle fibers *in situ*," J. Biomed. Opt. **9**(5), 882–892 (2004).
18. G. Recher, D. Rouède, P. Richard, A. Simon, J.-J. Bellanger, and F. Tiaho, "Three distinct sarcomeric patterns of skeletal muscle revealed by SHG and TPEF microscopy," Opt. Express **17**(22), 19763–19777 (2009).
19. G. Recher, D. Rouède, C. Tascon, L. A. D'Amico, and F. Tiaho, "Double-band sarcomeric SHG pattern induced by adult skeletal muscles alteration during myofibrils preparation," J. Microsc. **241**(2), 207–211 (2011).
20. F. Tiaho, G. Recher, and D. Rouède, "Estimation of helical angles of myosin and collagen by second harmonic generation imaging microscopy," Opt. Express **15**(19), 12286–12295 (2007).
21. E. Ralston, B. Swaim, M. Czapiga, W. L. Hwu, Y. H. Chien, M. G. Pittis, B. Bembi, O. Schwartz, P. Plotz, and N. Raben, "Detection and imaging of non-contractile inclusions and sarcomeric anomalies in skeletal muscle by second harmonic generation combined with two-photon excited fluorescence," J. Struct. Biol. **162**(3), 500–508 (2008).
22. I. Agarkova, E. Ehler, S. Lange, R. Schoenauer, and J. C. Perriard, "M-band: a safeguard for sarcomere stability?" J. Muscle Res. Cell Motil. **24**(2/3), 191–203 (2003).
23. R. Horowits, E. S. Kempner, M. E. Bisher, and R. J. Podolsky, "A physiological role for titin and nebulin in skeletal muscle," Nature **323**(6084), 160–164 (1986).
24. R. W. Ogilvie, R. B. Armstrong, K. E. Baird, and C. L. Bottoms, "Lesions in the rat soleus muscle following eccentrically biased exercise," Am. J. Anat. **182**(4), 335–346 (1988).
25. S. G. Page, and H. E. Huxley, "Filament Lengths in Striated Muscle," J. Cell Biol. **19**(2), 369–390 (1963).
26. J. L. Thompson, E. M. Balog, R. H. Fitts, and D. A. Riley, "Five myofibrillar lesion types in eccentrically challenged, unloaded rat adductor longus muscle--a test model," Anat. Rec. **254**(1), 39–52 (1999).
27. K. König, H. Liang, M. W. Berns, and B. J. Tromberg, "Cell damage in near-infrared multimode optical traps as a result of multiphoton absorption," Opt. Lett. **21**(14), 1090–1092 (1996).
28. K. König, T. W. Becker, P. Fischer, I. Riemann, and K. J. Halbhuber, "Pulse-length dependence of cellular response to intense near-infrared laser pulses in multiphoton microscopes," Opt. Lett. **24**(2), 113–115 (1999).
29. K. König, P. T. So, W. W. Mantulin, and E. Gratton, "Cellular response to near-infrared femtosecond laser pulses in two-photon microscopes," Opt. Lett. **22**(2), 135–136 (1997).
30. D. Linde, and H. Schüler, "Breakdown threshold and plasma formation in femtosecond laser solid interaction," J. Opt. Soc. Am. B **13**(1), 216–222 (1996).
31. J. Eng, R. M. Lynch, and R. S. Balaban, "Nicotinamide adenine dinucleotide fluorescence spectroscopy and imaging of isolated cardiac myocytes," Biophys. J. **55**(4), 621–630 (1989).
32. J. De Ruyck, M. Famerée, J. Wouters, E. A. Perpète, J. Preat, and D. Jacquemin, "Towards the understanding of the absorption spectra of NAD(P)H/NAD(P)+ as a common indicator of dehydrogenase enzymatic activity," Chem. Phys. Lett. **450**(1–3), 119–122 (2007).
33. W. Ying, "NAD+/NADH and NADP+/NADPH in cellular functions and cell death: regulation and biological consequences," Antioxid. Redox Signal. **10**(2), 179–206 (2008).
34. C. J. Bertling, F. Lin, and A. W. Girotti, "Role of hydrogen peroxide in the cytotoxic effects of UVA/B radiation on mammalian cells," Photochem. Photobiol. **64**(1), 137–142 (1996).
35. P. E. Hockberger, T. A. Skimina, V. E. Centonze, C. Lavin, S. Chu, S. Dadras, J. K. Reddy, and J. G. White, "Activation of flavin-containing oxidases underlies light-induced production of H2O2 in mammalian cells," Proc. Natl. Acad. Sci. U.S.A. **96**(11), 6255–6260 (1999).
36. J. M. Squirrell, D. L. Wokosin, J. G. White, and B. D. Bavister, "Long-term two-photon fluorescence imaging of mammalian embryos without compromising viability," Nat. Biotechnol. **17**(8), 763–767 (1999).
37. K. König, H. Liang, M. W. Berns, and B. J. Tromberg, "Cell damage by near-IR microbeams," Nature **377**(6544), 20–21 (1995).
38. D. Träutlein, M. Deibler, A. Leitenstorfer, and E. Ferrando-May, "Specific local induction of DNA strand breaks by infrared multi-photon absorption," Nucleic Acids Res. **38**(3), e14 (2010).
39. H. Oehring, I. Riemann, P. Fischer, K. J. Halbhuber, and K. Konig, "Ultrastructure and reproduction behaviour of single CHO-K1 cells exposed to near infrared femtosecond laser pulses," Scanning **22**(4), 263–270 (2000).

1. Introduction

Second-harmonic generation (SHG) imaging microscopy relies on a nonlinear interaction of tightly focused ultrashort infrared (IR) laser pulses with noncentrosymmetric quasi-crystalline arrangement of optically hyperpolarizable molecules (harmonophores) causing scattered coherent radiation at twice the fundamental frequency [1]. SHG is essentially an instantaneous phenomenon compared to fluorescence and all the incoming energy is

#139325 - $15.00 USD Received 7 Dec 2010; revised 14 Jan 2011; accepted 14 Jan 2011; published 19 Jan 2011

converted into scattered photons. The nonlinear nature of this optical process requires high peak intensities (GW to TW.cm^{-2} for femtosecond laser) that may induce photodamage and irreversible sample modifications when used above a certain threshold [2,3].

Alternatively, the high-peak intensities, high-spatial selectivity and confinement to subfemtoliter focal volume of two-photon excitation (TPE) [4,5] has been exploited in cell biology for photo-activation of single molecule [6], fluorescence photo-bleaching recovery [7] cell transfection consecutive to plasma-membrane permeabilization [8], nanodissection of human chromosome [9] reactive oxygen species (ROS) production [9,10] and photodynamic therapy [11].

In contrast to several studies considering DB sarcomeric SHG patterns as the main feature in skeletal muscle [1,12–17], we have shown that the predominant feature of sarcomeric SHG pattern is SB in physiological condition [18] and that this pattern is converted to DB during proteolysis, mechanical and chemical stresses [19]. In this report, we took advantage of supra GW peak intensities delivered by femtosecond IR laser to demonstrate *in situ* direct time lapse photo-conversion of physiological sarcomeric SB SHG pattern into DB indicating that this latter pattern should be considered as a signature of sarcomere alteration. The increase in DB sarcomeric pattern was mimicked and enhanced by the oxidant agent hydrogen peroxide (H_2O_2). The possible involvement of ROS production as a mediator of this nonlinear photo conversion is discussed.

2. Experimental methods

2.1 Tissue preparation

Premetamorphic stage 48-55 *Xenopus laevis* tadpoles (national breeding facility of xenopus animals in Rennes, France) were anesthetized in MS222 (0.5 mg.mL^{-1}). They were used either fresh in appropriated saline medium, or fixed with 4% paraformaldehyd (PFA) at 4°C overnight. For SHG imaging, the tails were cut and mounted in the imaging chamber (POC System, Pecon), in Mark's Modified Ringer (MMR), stabilized between two coverslips.

2.2 Imaging system

Images were acquired on PIXEL (http://pixel.univ-rennes1.fr/) facility of GIS EUROPIA, (University of Rennes1, France) based on a Leica TCS SP2 confocal scanning head coupled to a DMIRE2 inverted microscope and equipped with an IR 80 MHz femtosecond laser (MAITAI, Spectra Physics).

The laser beam was focalized through a water immersion 1.1 NA objective (LUMFl 60XW, Olympus). A motorized rotation stage (PR50CC, Newport) equipped with an achromatic zero-order Quartz-MgF_2 half-wave plate was used in order to adjust the mean power of the laser beam at the sample. The SHG signal was collected in a forward direction using a 0.90 NA multi-immersion condenser (model 501000, Leica). A BG39 bandpass filter and a 470 ± 5 nm interference filter were placed in front of the PMT.

2.3 Image acquisition protocol

We measured the PSF (point spread function) using 0.17 µm subresolution fluorescent beads and we found 0.44 µm and 2.0 µm of FWHM respectively for lateral and axial resolution. In most measurements, the laser power at the output of the objective lens was 27-50 mW, corresponding to peak power densities of 1.1- 2.0 TW.cm^{-2}.

All images were acquired using either a single (pre-conversion step) or a time-lapse frame protocol (photo-conversion step) from 3 to 5 different tadpoles and 7-12 different randomly chosen fields. During the pre-conversion step, a 30 X 30 µm^2 randomly chosen field of view is scanned during 10 s (512 X 512 pixels, 4 lines-averages, 10 µs pixel dwell time). During the photo-conversion step, the previous field of view is zoomed by a factor of 2 (15 X 15 µm^2). A time lapse sequence is performed up to 10 min. Each frame of the time lapse last 20 s (512 X 512 pixels, 8 lines-averages, 10 µs pixel dwell time). Thus the energy deposition is 8 fold higher than in the pre-conversion step. Each measurement was performed at both 780

#139325 - $15.00 USD Received 7 Dec 2010; revised 14 Jan 2011; accepted 14 Jan 2011; published 19 Jan 2011

and 940 nm excitation wavelengths. The images were acquired from muscle tissues localized at depth 150-200 µm below the skin surface of each tadpole. Because of light scattering the focalized intensity decreases with the depth inside the sample. To compensate for this effect we adjusted the IR power to obtain the same SHG image intensity deep inside the sample as close to the surface, while the PMT voltage was kept constant.

2.4 Image and data analysis

The images were analyzed with the open source ImageJ software (http://rsb.info.nih.gov/ij/). A Gaussian blur filter of a 2 pixels radius was first applied to each image.

The proportion of SB and DB sarcomeric SHG patterns were quantified for each frame using pixel intensity profile analysis along myofibrils main axis [18] and the half-time latency ($\tau_{1/2}$) corresponding to 50% of SB to DB conversion was determined for the time lapse protocol.

Average sarcomere size was obtained along randomly chosen lines covering 6 – 10 sarcomeres. This value was determined for a number $n>10$ of randomly chosen fields for each experimental condition and the mean of these averages was calculated.

3. Results

We checked that the pre-conversion acquisition protocol did not alter the sarcomeric SHG pattern for two excitation wavelengths, namely 780 and 940 nm. The result is shown in Fig. 1(a) for 780 nm excitation wavelength. The intensity profile analysis of the sarcomeric SHG signal resulted in 98 ± 5% (n = 12) and 93 ± 7% (n = 8) predominant SB sarcomeric SHG pattern respectively for 780 and 940 nm excitation wavelength, as quantified in Table 1. These results are in agreement with our previous reports [18,19]. Repeating the pre-conversion protocol every 26 s, for 10 min did not affected the sarcomeric SHG patterns (data not shown). This latter protocol was not repeated for all further experiments.

However, the photo-conversion protocol, corresponding to an 8 fold increase in energy deposition compared to the pre-conversion protocol (see Experimental Methods section) was found to induce a spatiotemporal SB to DB sarcomeric SHG pattern conversion (Fig. 1) but only for the 780 nm excitation wavelength, as quantified in Table 1. The appearance of sarcomeric DB induced by the 780 nm excitation wavelength is similar to the effect that we have previously observed in muscle during proteolysis, mechanical and chemical stresses [18,19]. All the sarcomeres in the imaging field of view were always fully converted into DB SHG pattern in less than 10 min. The half-time latency ($\tau_{1/2}$) for 50% SB to DB conversion was found to vary between 52 s and 4 min (Fig. 2) and the average calculated value for 12 different fields from 4 tadpoles was 2,17 min ± 8 s (Table 1). We found that the slight apparent decrease in sarcomere size during the SB to DB photo-conversion (Table 1) was not significant, therefore excluding the rise in intracellular calcium, a contraction inducer, as the trigger of this photo-conversion process. We also performed a polarization dependent study of the SHG intensity profile before and after photoconversion. The effective orientation angle θ of the harmonophores relative to the myofibril main axis was found to be respectively 62 ± 1 (n = 5) and 61 ± 1 (n = 6) for pre and post conversion measurements. This value corresponds to the pitch angle of the single α helix of myosin, in agreement with our previous finding [20] indicating no significant difference of the orientation of the harmonophores. Conversion of SB to DB is often followed by contrast reduction as shown in Fig. 1(d) suggesting a decrease of the density of the harmonophores. We often noticed that the SB to DB conversion was slightly propagated beyond the zoom area in an anisotropic manner, following the long axis of myofibrils (Fig. 1(b)).

When the same photo-conversion protocol was applied at 940 nm excitation with similar mean powers, no significant SB to DB conversion was observed for times up to 10 min of recording as quantified in the Table 1.

#139325 - $15.00 USD Received 7 Dec 2010; revised 14 Jan 2011; accepted 14 Jan 2011; published 19 Jan 2011

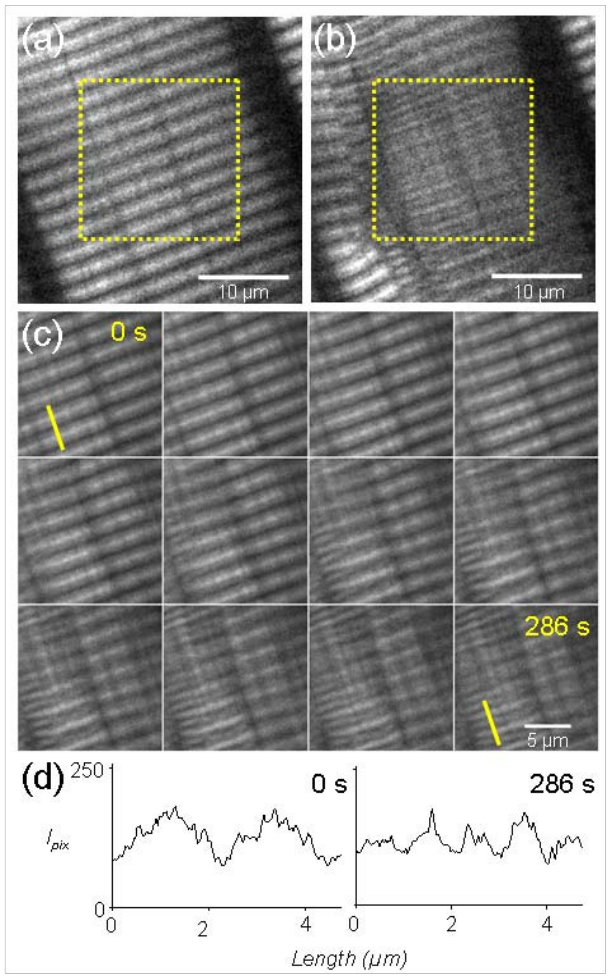

Fig. 1. Typical SHG images illustrating the laser-induced SB to DB sarcomeric SHG pattern conversion obtained at 780 nm excitation wavelength. (a) and (b) are examples of pre- and post-conversion single frame protocol images obtained respectively before and after the photo-conversion time-lapse protocol (c) (see Experimental Methods section). In (c), thumbnail strips are representative of the photo-conversion time-lapse sequence (left- right and top-down) and were realized in the dot-delimited area in (a) and (b). (d) Raw pixels intensity (I_{pix}) profiles (8-bit scale) along indicated lines in the first and the last frames in (c). Note that the first and last thumbnail and their corresponding intensity profiles at indicated lines are labeled "0 s" and "286 s" which correspond to their acquisition time within the sequence. Note the progressive spatiotemporal (left to right) "wave-like" propagation of sarcomere SHG pattern duplication within the sequence. Both thumbnail and intensity profile plots indicate a great contrast reduction suggestive of photodamage. This photodamage is accompanied by a SB to DB conversion which was slightly propagated beyond the zoom area in (b) in an anisotropic manner, following the long axis of myofibrils.

Altogether these results suggest that sarcomeric SHG pattern photo-conversion is obtained selectively for 780 nm excitation wavelength and for peak power at the output of the objective of 1.1–2.0 TW.cm^{-2}.

Following Hopth et al. [2] we assume that photo-conversion manifests itself when noxious substance, generated at rate r_D, surpasses a certain threshold concentration

$$C_{th} \propto r_D \tau_{th}. \quad (1)$$

#139325 - $15.00 USD Received 7 Dec 2010; revised 14 Jan 2011; accepted 14 Jan 2011; published 19 Jan 2011

Table 1: Quantification of sarcomeric SHG signals in different experimental conditions as indicated in the table[a]

		780 nm		940 nm	
		Protocol 1	Protocol 2	Protocol 1	Protocol 2
Control	SB (%)	98 ± 5	0 ± 0	93 ± 7	92 ± 6
	$\tau_{1/2}$ (min)		2.17 ± 0.13		
	Sarcomere size (µm)	2.16 ± 0.04	2.08 ± 0.09	2.18 ± 0.03	2.23 ± 0.04
PFA	SB (%)	95 ± 4	95 ± 4	nd	nd
	Sarcomere size (µm)	2.39 ± 0.08	2.41 ± 0.06	nd	nd
H_20_2	SB (%)	58 ± 6	0 ± 0	72 ± 8	53 ± 6
	$\tau_{1/2}$ (min)		0.41 ± 0.02		> 10
	Sarcomere size (µm)	2.25 ± 0.05	2.17 ± 0.10	2.29 ± 0.08	2.24 ± 0.11

[a]Protocol 1 and protocol 2 correspond respectively to single frame pre-conversion and time lapse photo-conversion protocols defined in Experimental Methods section. The H_20_2 and PFA recordings conditions correspond to tadpoles that respectively received 5 µL of hydrogen peroxide (90 mM) injected in the heart and have been fixed in parafolmadehyd (see Experimental Methods section). The three lines of each experimental condition (control, PFA and H_20_2) have the following meaning. Mean percentage and standard error of the mean (± SEM) of SB sarcomeres; half-time latency ($\tau_{1/2}$) for 50% SB to DB sarcomeric SHG pattern conversion; mean size and standard deviation (± STD) of sarcomeres; the mean percentage has been determined using intensity profile analysis (18); "nd" means not determined.

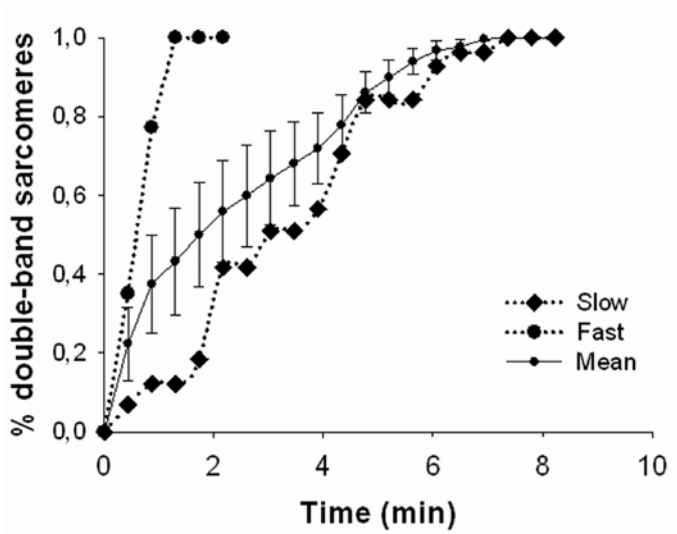

Fig. 2. Kinetic of laser-induced SB to DB sarcomeric SHG pattern photo-conversion. Percentages of DB were determined from the photo-conversion time lapse protocol (see Experimental Methods section). Filled circle without error bars, filled diamond without error bars and filled circle with error bars represent data respectively from the fastest, slowest and average kinetics observed.

In Eq. (1) τ_{th} represents the time to reach the threshold concentration. Unlike Hopth et al. [2], we deduced from Fig. 2 that r_D is not a constant and its value might depend on the spatial position of each sarcomere. Therefore τ_{th} is proportional to $\tau_{1/2}$. Assuming that the noxious substance is generated as a multiphoton process we have $r_D \propto I^{\upsilon}$, then the dependency of $\tau_{1/2}$ with incident laser power *I* follows:

$$\log(\tau_{1/2}) = cste - \upsilon \log(I). \quad (2)$$

We next determined the log-log relationship between the half-time latency (($\tau_{1/2}$)) to sarcomeric SHG pattern photo-conversion and the laser power intensity (I) at the output of

#139325 - $15.00 USD Received 7 Dec 2010; revised 14 Jan 2011; accepted 14 Jan 2011; published 19 Jan 2011

the objective lens (Eq. (2)). The slope of the best linear regression fit of the data points yield the nonlinear power order υ = 3.1 (Fig. 3) which is close to υ = 2.5 found for photodamage observed in neurons [3] and bovine adrenal chromaffin cells [2]. Incidentally, as expected for a two-photon nonlinear optical process, the log-log plot of the SHG and auto-fluorescence intensities as a function of the laser power intensity (I) yielded υ values of respectively 1.9 and 2.0 (data not shown).

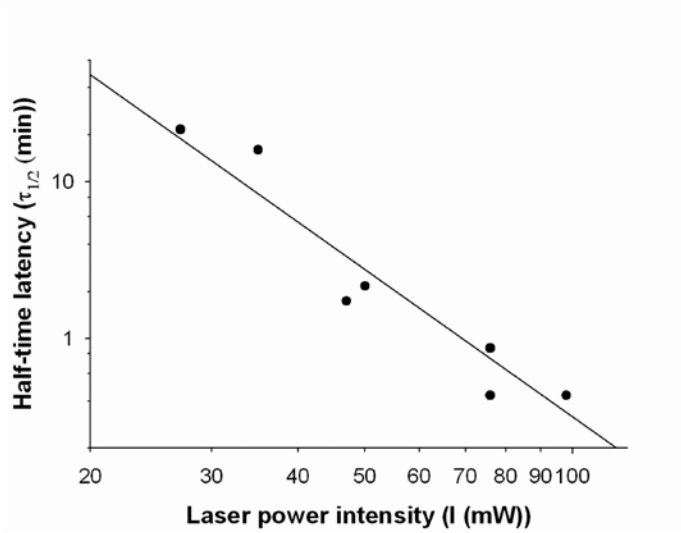

Fig. 3. Influence of the laser mean power intensity (I) on SB to DB sarcomeric SHG pattern photo-conversion kinetic. The incident laser power was varied and the half-time ($\tau_{1/2}$) until 50% SB to DB conversion was determined. Each symbol represents value from distinct field of view. Care was taken to maintain the focal plane at the same z position within the sample. The logarithm of the half-time latency $\tau_{1/2}$ was plotted against the logarithm of the laser power intensity (I) at the output of the objective lens. Fits were obtained by linear regression with the following equation: $\log(\tau_{1/2}) = 5.8 - 3.1\log(I)$; R = 0.94.

We further asked whether a vital biochemical mechanism could be involved in this process. To this aim, tadpoles were fixed in PFA 4% to prevent these biochemical mechanisms. In this condition, when the photo-conversion time lapse protocol was applied, the sarcomeric SHG pattern remained predominantly SB at 780 nm as quantified in Table 1 and therefore these experiments were not extended at 940 nm.

Since it has been shown that near IR laser at mean power above 7 mW could induced ROS [9,10], we tested the hypothesis that ROS could mediate the laser-induced SB to DB conversion. To this aim, tadpoles were injected with 5 µL of 90 mM hydrogen peroxide (H_2O_2) diluted in MMR and sarcomeric SHG images were recorded at least 30 min later. For pre-conversion single frame protocol, we found that tadpoles injected with H_2O_2 had significant SB to DB conversion as illustrated in Fig. 4 and Fig. 5. The proportion of SB sarcomeres was 58% (n = 7) for a 780 nm excitation and 72% (n = 8) for 940 nm. These results are distinct from those obtained in the absence of H_2O_2 and from our previous report [18,19]. Applying the photo-conversion time lapse protocol in the presence of H_2O_2 results in a half-time latency $\tau_{1/2}$ of laser-induced SB to DB conversion that was drastically reduced at 780 nm ($\tau_{1/2}$ = 24 ± 11 s). $\tau_{1/2}$ was longer and not measurable in most experiments at 940 nm during the 10 min time lapse protocol; however the proportion of SB dropped from 72 to 53%, as illustrated in Fig. 4, yielding an estimated $\tau_{1/2}$ of 23 min. We also found during this time lapse protocol, a great attenuation of the SHG signal at 780 nm as shown in Fig. 5(d) indicating a significant reduction of the density of the underlying single α helix of myosin packed in thick filaments [20]. The average relative reduction of the SHG signal for 10 min exposition was found to be 95 ± 3%. We noticed that the laser-induced SB to DB conversion

#139325 - $15.00 USD Received 7 Dec 2010; revised 14 Jan 2011; accepted 14 Jan 2011; published 19 Jan 2011

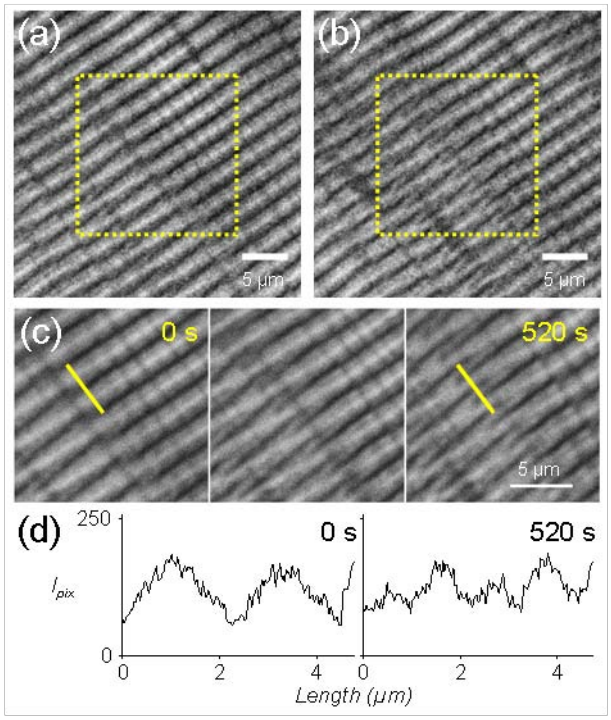

Fig. 4. Laser-induced alteration of sarcomeric SHG pattern at 940 nm excitation in the presence of hydrogen peroxide (5 µL, 90 mM) injected in the heart of tadpoles. (a) and (b) are examples of pre- and post-conversion single frame protocol images obtained respectively before and after the photo-conversion time lapse protocol (c) (see Experimental Methods section). (c) Thumbnail strips representative of the photo-conversion time lapse sequence (from left to right) realized in the dot-delimited area in (a) and (b).(d) Raw pixels intensity (I_{pix}) profiles (8-bit scale) along indicated lines in the first and the last frames. Note that the first and last thumbnail and their corresponding intensity profiles are labeled "0 s" and "520 s" which correspond to their acquisition time within the sequence.

was extended out of the laser scanned area. This propagation was anisotropic, was quite parallel to the myofibril axis and limited as illustrated in Fig. 5(b).

Altogether these results suggest that the laser-induced SB to DB sarcomeric pattern photo-conversion could involve laser-induced production ROS as a prerequisite of muscle thick filaments disorganization and degradation.

4. Discussion

The main finding reported in this study is that 780 nm excitation wavelength at peak power of 1.1 – 2.0 $TW.cm^{-2}$ at the output of the objective could be used to photo-convert the sarcomeric SB SHG pattern into DB in *Xenopus laevis* premetamorphic tail muscles. This photo-conversion was found to be a third order nonlinear process and was enhanced in the presence of hydrogen peroxide but was drastically reduced at 940 nm excitation wavelength. This effect was no longer observed in PFA fixed muscles.

This sarcomeric SHG pattern photo-conversion is an indication of muscle alteration in agreement with previous report implicating muscles proteolysis, mechanical and chemical stress [18,19] and disease induced muscular lesions [21]. The selective SB to DB sarcomeric SHG pattern photo-conversion observed at 780 nm could be due to the destruction of the elastic titin molecule and M-band proteins involved respectively in centering and aligning myosin thick filaments with regards to Z-discs [22]. Misalignment of thick filaments has already been observed in eccentric contractions at the ultra-structural level [23–26]. The

#139325 - $15.00 USD Received 7 Dec 2010; revised 14 Jan 2011; accepted 14 Jan 2011; published 19 Jan 2011

observed DB sarcomeric SHG pattern might be due to thick filaments misalignment resulting in inter-thick filaments centrosymmetry at the A-band as previously suggested [18]. The functional consequence of this DB sarcomeric SHG pattern should therefore be a decrease of both active and passive sarcomeric mechanical tension as was already demonstrated with ionizing radiations induced muscle titin degradation [23].

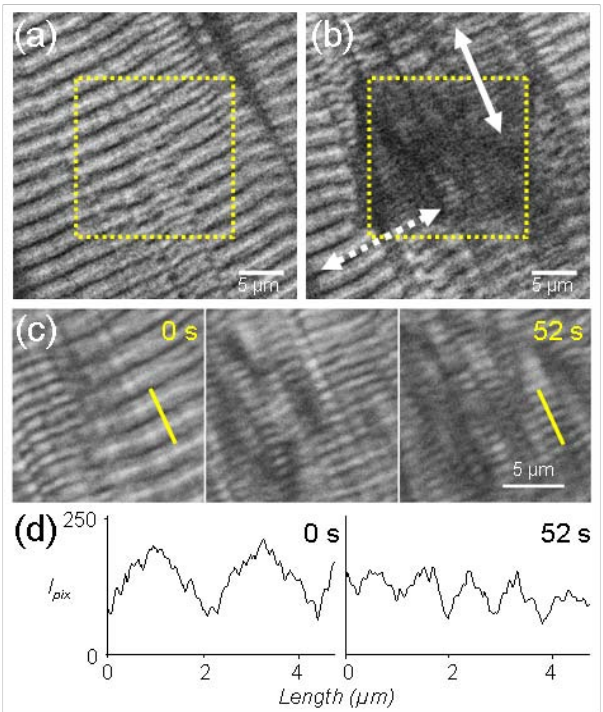

Fig. 5. Laser-induced alteration of sarcomeric SHG pattern at 780 nm excitation in the presence of hydrogen peroxide (5 µL, 90 mM) injected in the heart of tadpoles. (a) and (b) are examples of pre- and post-conversion single frame protocol images obtained respectively before and after the photo-conversion time lapse protocol (c) (see Experimental Methods section). (c) Thumbnail strips representative of the photo-conversion time lapse sequence (from left to right) realized in the dot-delimited area in (a) and (b). (d) Raw pixels intensity (I_{pix}) profiles (8-bit scale) along indicated lines in the first and the last frames are presented below the strips. Note that the first and last thumbnail and their corresponding intensity profiles are labeled "0 s" and "52 s" which correspond to their acquisition time within the sequence. Note the dark central zone of (b) corresponding to the dot-delimited area scanned during the photo-conversion time lapse protocol. The double headed continuous and dotted arrows represent respectively the favorable and unfavorable propagation direction of the effect of the laser outside the scanned area. Note that the propagation direction is quite parallel to the myofibril axis.

The photo-conversion of sarcomeric SHG pattern reported in this study is reminiscent of previous photodamages observed at mean powers above 7 mW (at the cell level) in different cell types. These photodamages concerned red blood cell lysis [27], Chinese hamster ovarian (CHO) cells division impairment [28,29], rise in basal neuronal dendrites fluorescence [3] and abrupt rise in basal [Ca^{2+}] in bovine adrenal chromaffin cells [2]. The SB to DB sarcomeric SHG pattern photo-conversion was selectively pronounced at 780 nm excitation wavelength and greatly reduced at 940 nm. This selectivity is in full agreement with previous wavelength-dependent photodamage reported for CHO cell division [28]. Single IR photon absorption induced photo-thermal effects are excluded to explain the photo-conversion of sarcomeric SHG pattern since (1) the power dependency of the effect is nonlinear (power order $\upsilon = 3$), (2) the effect is reduced at 940 nm compare to 780 nm, (3) was not isotropic and (4) was not observed in PFA fixed muscles. This conclusion is in agreement with the

#139325 - $15.00 USD Received 7 Dec 2010; revised 14 Jan 2011; accepted 14 Jan 2011; published 19 Jan 2011

nonlinear photodamage reported in CHO cells [28], bovine adrenal chromaffin cells [2] and basal neuronal dendrites [3]. Laser-induced plasma formation [29,30] is also excluded (1) considering the reasons mentioned above, (2) the peak power is below the 10 $TW.cm^{-2}$ threshold reported [30] and (3) significant photodamage at 940 nm was observed only in the presence of hydrogen peroxide suggesting the involvement of a biochemical process.

We found that the laser-induced sarcomeric SHG pattern photo-conversion could be extended out of the scanning area parallel to myofibrils axis (see Fig. 5(b)), in the vicinity of regions where mitochondria use to be localized [31], suggesting their possible involvement in this laser-induced photo-conversion. A power order $\upsilon = 3$ suggests that the endogenous photosensitizer involved in this photo-conversion might be a nonlinear three photons absorber. For an efficient laser power of 780 nm, this implies that the photosensitizer might have a single photon absorption wavelength of about 260 nm. Known abundant endogenous single photon absorber at this wavelength could be NAD/NADPH or NADP/NADPH that mainly localized in mitochondria [31,32]. The oxidized NAD and NADP are not fluorescent in contrast to NADH and NADPH and they could contribute to photochemical reactions leading to the accumulation of an intracellular noxious substance like ROS (for review see [33]). For a photosensitizer absorbing at about 260 nm, a laser wavelength of 940 nm would necessitate an efficient four order nonlinear process to produce the noxious substance. This would imply higher peak power densities (largely above $TW.\ cm^{-2}$) that we did not achieve in our recording condition, explaining why this longer wavelength was not efficient in inducing SB to DB photo-conversion.

It has been proposed that non linear IR laser photodamage might be related to time-dependent accumulation of noxious substance at suprathreshold peak powers [2]. In this model, the rate of this noxious substance accumulation depends on the exposure time. Considering this model, at suprathreshold peak powers the sarcomeric dwell time might be a key factor involved in the observed alteration of the sarcomeric SHG signal. It is therefore the switch from pre-conversion single frame to photo-conversion time-lapse protocol at constant peak power density resulting in 8 fold increase in sarcomere dwell time that enables the efficient accumulation of the noxious substance. Interestingly the significant increase in DB sarcomeric SHG pattern observed during the pre-conversion single frame protocol in the presence of H_2O_2 both at 780 and 940 nm combined to the reduced $\tau_{1/2}$ of laser-induced conversion of SB to DB suggest that oxidative stress could mediate this photo-conversion. The relation between oxidative stress, ROS production and photodamage has been highlighted in previous experiments with either single UV photon absorption [34–36] or two-photon near IR absorption processes [9,37,38]. We observed a spatial variation in the kinetics of SB to DB photo-conversion (Fig. 1 and Fig. 2) with half-time latency from few seconds to several minutes indicating that the rate constant of accumulation of the noxious substance is spatially modulated. The anisotropic propagation of the laser-induced SB to DB sarcomeric SHG pattern conversion shown in Fig. 5 suggests that the biochemical subtract of ROS production might be compartmentalized and propagated outside the scanned area. Such extension of the photodamage outside the laser scanning area has been observed in dendrites of neurons (3). Interestingly it has been shown, in CHO cells, that laser-induced photodamage leads to increase auto-fluorescence of coenzyme-rich mitochondria [29] or their complete destruction [39] suggesting that mitochondria might be the cell compartment involved in ROS production.

This is the first report to our knowledge showing the modulation of sarcomeric SHG pattern by high intensity femtosecond laser illumination resulting in the conversion from predominant SB in physiological condition to DB after photodamage in xenopus tadpole tail muscles. The possible involvement of ROS is this photoconversion suggest that modulation of sarcomeric SHG patterns could be a useful marker for investigating oxidative stress effects in muscle function and diseases.

#139325 - $15.00 USD Received 7 Dec 2010; revised 14 Jan 2011; accepted 14 Jan 2011; published 19 Jan 2011

Acknowledgments

We thank Région Bretagne, Rennes Métropole, Conseil Général d'Ille-et-Vilaine and Ministère de l'enseignement supérieur et de la recherche for their financial support, and Matthieu Fabrega for his technical help.

#139325 - $15.00 USD Received 7 Dec 2010; revised 14 Jan 2011; accepted 14 Jan 2011; published 19 Jan 2011